Conformational flexibility and inhibitor binding to unphosphorylated interleukin-1 receptor–associated kinase 4 (IRAK4)

Received for publication, August 19, 2018, and in revised form, January 21, 2019 Published, Papers in Press, January 24, 2019, DOI 10.1074/jbc.RA118.005428

Li Wang[‡§1], **Ryan Ferrao**[‡§1], **Qiubai Li**[‡§], **John M. Hatcher**[‡¶], **Hwan Geun Choi**[‡¶], **Sara J. Buhrlage**[‡¶], **Nathanael S. Gray**[‡¶], and **Hao Wu**[‡§2]

From the [‡]*Department of Biological Chemistry and Molecular Pharmacology, Harvard Medical School, Boston, Massachusetts 02115, the* [§]*Program in Cellular and Molecular Medicine, Boston Children's Hospital, Boston, Massachusetts 02115, and the* [¶]*Department of Cancer Biology, Dana-Farber Cancer Institute, Boston, Massachusetts 02115*

Edited by Wolfgang Peti

Interleukin-1 receptor–associated kinase 4 (IRAK4) is a key player in innate immune and inflammatory responses, performing a critical role in signal transduction downstream of Toll-like receptors and interleukin-1 (IL-1) receptors. Upon ligand binding and via its N-terminal death domain, IRAK4 is recruited to an oligomeric receptor that is proximal to the Myddosome signaling complex, inducing IRAK4 kinase domain dimerization, autophosphorylation, and activation. To date, all known IRAK4 structures are in the active conformation, precluding a good understanding of IRAK4's conformational dynamics. To address this issue, here we first solved three crystal structures of the IRAK4 kinase domain (at ≤2.6 Å resolution), in its unphosphorylated, inactive state bound to either the ATP analog AMP-PNP or to one of the two small-molecule inhibitors JH-I-25 and JH-I-17. The structures disclosed that although the structure in complex with AMP-PNP is in an "αC-out" inactive conformation, those in complex with type I inhibitors assume an active "Asp–Phe–Gly (DFG)-in" and "αC-in" conformation. The ability of unphosphorylated IRAK4 to take on variable conformations prompted us to screen for small-molecule inhibitors that bind preferentially to unphosphorylated IRAK4, leading to the identification of ponatinib and HG-12-6. Solving the structures of unphosphorylated IRAK4 in complex with these two inhibitors, we found that they both bind as type II inhibitors with IRAK4 in a "DFG-out" conformation. Collectively, these structures reveal conformational flexibility of unphosphorylated IRAK4 and provide unexpected insights into the potential use of small molecules to modulate IRAK4 activity in cancer, autoimmunity, and inflammation.

Toll-like receptors (TLRs)[3] and Interleukin-1 (IL-1) receptors perform critical roles in innate immune and inflammatory responses (1, 2). Ligand binding to these receptors initiates the assembly of the Myddosome, a complex comprised of the MyD88 adapter protein and the IRAK family of kinases (3, 4). The IRAK kinases are multidomain proteins whose N-terminal death domains (DDs) facilitate their recruitment to the Myddosome complex via DD–DD interactions (3). IRAK4 is the most upstream kinase in this pathway and associates directly with MyD88, an essential interaction for Myddosome formation. Myddosome assembly triggers dimerization of the IRAK4 kinase domain and *trans*-autophosphorylation of the IRAK4 activation loop (5). Active IRAK4 phosphorylates and activates the downstream kinases IRAK1 and IRAK2, leading to activation of the ubiquitin–protein isopeptide ligase TRAF6, which in turn promotes transforming growth factor β-activated kinase 1 and inhibitor of κB kinase recruitment and activation (1, 6). Transforming growth factor β-activated kinase 1 and inhibitor of κB kinase then phosphorylate the inhibitor IκB, enabling nuclear translocation of NF-κB transcription factors and subsequent gene transcription (1, 6).

The kinase activity of IRAK4 plays an important role in signal transduction downstream of TLRs and IL-1 receptors. Knockin mice homozygous for a kinase inactive IRAK4 are resistant to septic shock and exhibit defective cytokine production in response to IL-1β, as well as the TLR agonists lipopolysaccharide and CpG oligodeoxynucleotide (7, 8). In humans, deficiency of either MyD88 or IRAK4 renders the patient susceptible to invasive pyogenic infections (9, 10). Loss of IRAK4 kinase activity has been shown to result in decreased Aβ levels and amyloid plaque burden in mouse models of Alzheimer's disease (11). Mouse models have also implicated IRAK4 kinase activity in disease progression of atherosclerosis (12) and rheumatoid arthritis (13). Signaling through the MyD88-IRAK4 pathway has also been shown to play a role in cancer. Gain of function MyD88 mutations are prevalent in diffuse large B-cell lymphoma and Waldenström's macroglobulinemia (14, 15).

This work was supported by the National Institutes of Health Grant AI050872 (to H. W.). Although the work was performed solely in academia, Ryan Ferrao and Li Wang are currently employees of Gilead Sciences and SMOC Therapeutics, respectively. The content is solely the responsibility of the authors and does not necessarily represent the official views of the National Institutes of Health.

This article contains Table S1 and Figs. S1–S5.

The atomic coordinates and structure factors (codes 6EGF, 6EGD, 6EGE, 6EGA, and 6EG9) have been deposited in the Protein Data Bank (http://wwpdb.org/).

[1] These authors contributed equally to this work.

[2] To whom correspondence should be addressed. E-mail: wu@crystal.harvard.edu.

[3] The abbreviations used are: TLR, Toll-like receptor; IL, interleukin; IRAK, IL-1 receptor–associated kinase; PDB, Protein Data Bank; AMP-PNP, adenosine 5′-(β,γ-imino)triphosphate; DD, death domain; CDK, cyclin-dependent kinase; EGFR, epidermal growth factor receptor; R-spine, regulatory spine.

Table 1
Crystallographic statistics
The numbers in parentheses are for the highest resolution shell.

PDB code	6EGF	6EGD	6EGE	6EGA	6EG9
Ligand	AMP-PNP	JH-I-17	JH-I-25	HG-12–6	Ponatinib
Construct	Arg^{164}–Ser^{460} (D311N)	Arg^{164}–Ser^{460} (D311N)	Arg^{164}–Ser^{460} (D311N)	Arg^{164}–Ser^{460} (WT, dephosphorylated)	Arg^{164}–Ser^{460} (WT, dephosphorylated)
Structure determination	Molecular replacement	Molecular replacement	Molecular replacement	Molecular replacement	Molecular replacement
Data collection					
Beamline	APS 24-ID-C	NSLS X25A	NSLS X4A	APS 24-ID-C	APS 24-ID-E
Space group	$P6_322$	$P2_1$	$P2_1$	$P6_122$	$P6_122$
Cell dimensions					
a, *b*, *c* (Å)	135.2, 135.2, 126.4	71.6, 59.5, 75.6	70.9, 58.6, 76.1	84.6, 84.6, 429.0	84.9, 84.9, 433.9
α, β, γ (°)	90.0, 90.0, 120.0	90.0, 111.8, 90.0	90.0, 112.8, 90.0	90.0, 90.0, 120.0	90.0, 90.0, 120.0
Wavelength (Å)	0.98	1.10	0.98	0.98	0.98
Resolution (Å)	85.9–2.6 (2.7–2.6)	44.3–2.1 (2.2–2.1)	37.6–1.4 (1.5–1.4)	73.3–2.5 (2.6–2.5)	73.6–2.3 (2.4–2.3)
$CC_{½}$	1 (0.76)	1 (0.77)	1 (0.85)	1 (0.54)	1 (0.71)
R_{merge}	0.073 (1.73)	0.053 (0.93)	0.053 (0.92)	0.210 (1.86)	0.112 (2.32)
Mean $I/\sigma I$	26.3 (2.1)	21.2 (2.0)	17.8 (2.4)	21.7 (1.6)	22.5 (1.9)
Completeness (%)	99.8 (99.4)	99.3 (98.2)	98.1 (94.9)	99.4 (94.8)	100.0 (100.0)
Total reflections	405,129 (40,265)	228,850 (22,254)	833,848 (79,412)	1,143,455 (81,435)	1,050,373 (82,983)
Unique reflections	21,291 (2,079)	34388 (3,358)	110,700 (10,742)	32,497 (3,388)	50,049 (4,233)
Multiplicity	19.0 (19.4)	6.7 (6.6)	7.5 (7.4)	35.2 (24.0)	21.0 (19.6)
Refinement					
R_{work}/R_{free} (%)	20.5/22.9	18.4/22.9	17.8/20.2	27.2/29.8	21.0/24.6
Average B-factor ($Å^2$)	87.7	56.8	32.5	78.3	54.0
Proteins	88.1	57.1	31.7	78.4	63.0
Ligands	86.4	44.9	21.7	73.1	56.9
Root mean square deviations					
Bond lengths (Å)/angles (°)	0.01/0.44	0.01/1.11	0.01/1.17	0.006/1.11	0.01/1.31
Ramachandran plot, favored/outliers (%)	96.4/0.0	96.6/0.0	98.7/0.0	97.5/0.0	98.0/0.0

Reconstitution of activated diffuse large B-cell lymphoma lines with kinase inactive IRAK4 or inhibition with an IRAK1/4 inhibitor was lethal to cells (14). Taken together, these results make inhibition of IRAK4 an attractive therapeutic target.

Although IRAK4 kinase activity is greatly enhanced upon phosphorylation (5), the kinase must also possess the ability to adopt an active conformation in the absence of activation loop phosphorylation to allow for *trans*-autophosphorylation. Phosphorylation-independent kinase activation is typically induced by the binding of an allosteric activator protein to induce adoption of the active conformation. Rapidly accelerated fibrosarcoma kinases, cyclin-dependent kinases (CDKs), and the epidermal growth factor receptor (EGFR) family kinases are activated in this manner (16–18). For IRAK4, upon dimerization, one monomer adopts the active conformation and phosphorylates the activation loop of its partner (5). Understanding the transition between inactive and active protein kinase conformations is an important area of focus in the study of kinases (19, 20). However, no structures of inactive conformations of IRAK4 have been solved, leaving the regulatory mechanism obscured. Here we present five crystal structures of the unphosphorylated IRAK4 kinase domain in complex with AMP-PNP and four small molecule inhibitors. These structures reveal that unphosphorylated IRAK4 can adopt different conformations depending on the bound small molecule, suggesting its conformational flexibility. We hypothesize that targeting these specific conformations will aid in the development of highly potent and selective small molecule IRAK4 inhibitors for a variety of indications.

Results

Structure of the unphosphorylated IRAK4 kinase domain in complex with AMP-PNP

We expressed a construct containing the catalytically dead D311N mutant of $IRAK4^{KD}$ in insect cells and purified it to homogeneity as described previously (5). The protein was co-crystallized with the nonhydrolyzable ATP analog AMP-PNP and Mg^{2+}, and we determined its structure at 2.6 Å resolution (Table 1). A single $IRAK4^{KD\text{-}D311N}$ molecule comprises the asymmetric unit, and the electron density for the bound AMP-PNP in the active site was clearly visible (Fig. S1, *A* and *B*). Surprisingly, the overall conformation of the unphosphorylated $IRAK4^{KD}$ bound to AMP-PNP (Fig. 1*A*) was immediately distinguishable from previously solved structure of the phosphorylated, AMP-PNP–bound IRAK4 and other IRAK4 structures in an active conformation (Fig. 1*A*) (5, 26–34). In the phosphorylated $IRAK4^{KD}$, the αC helix is pulled in toward the active site, allowing for the formation of a catalytically important salt bridge between Glu^{233} and the active site residue Lys^{213} (Fig. 1*B*). In the current unphosphorylated IRAK4 structure, the N-terminal end of the αC helix is translated away from the active site by ~8 Å and rotated by ~20° along its axis, positioning Glu^{233} toward the activation loop and breaking the catalytically important salt bridge between Glu^{233} and the active site residue Lys^{213} ("αC-out") (Fig. 1, *A* and *B*).

The outward movement of the αC helix appears to be coupled to conformational changes in the activation loop and the Asp–Phe–Gly (DFG) motif. In phosphorylated IRAK4, the activation loop adopts an elongated conformation that is stabilized by a salt bridge between Arg^{334} and the phosphate group of $pThr^{345}$ (Fig. 1,

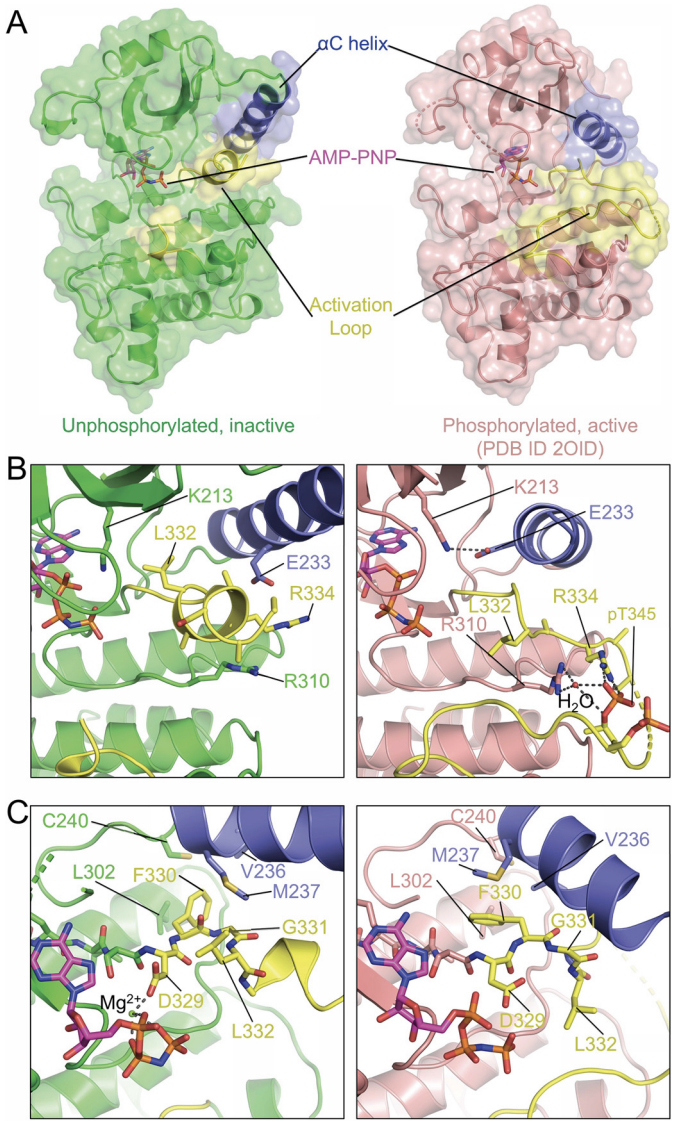

Figure 1. Structure of AMP-PNP bound IRAK4 kinase domain. *A*, cartoon representation of the unphosphorylated IRAK4 kinase domain in an inactive conformation in complex with AMP-PNP (*left*, *green*). AMP-PNP–bound phosphorylated IRAK4 in the active conformation (*right*, *pink*) (PDB code 2OID) is shown for comparison. The αC-helix and activation loop are colored *blue* and *yellow*, respectively. AMP-PNP (*magenta*) is shown as *sticks*. *B*, detailed comparison of the αC-helix and activation loop conformation between unphosphorylated (*left*, *green*) and phosphorylated (*right*, *pink*) IRAK4. *C*, detailed interactions between the DFG motif, αC-helix, and AMP-PNP in both the unphosphorylated (*left*, *green*) and phosphorylated (*right*, *pink*) IRAK4. In both *B* and *C*, the αC-helix, activation loop, and AMP-PNP are colored as in *A*.

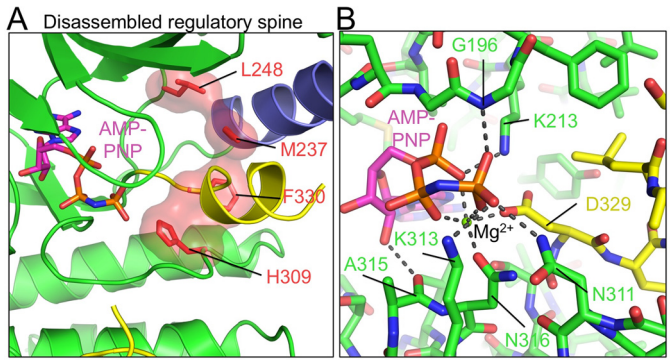

Figure 2. Regulatory spine of the AMP-PNP bound IRAK4 kinase domain structure. *A*, detailed view of the residues that form the regulatory spine, shown as *red sticks* and highlighted with *red surface*. The αC-helix and activation loop are colored *blue* and *yellow*, respectively. AMP-PNP (*magenta*) is shown in a *stick model*. Disassembled regulatory spine indicates an inactive conformation of IRAK4. *B*, detailed interactions between AMP-PNP (*magenta*), Mg^{2+}, and unphosphorylated IRAK4 (*green*). IRAK4 DFG motif is colored in *yellow*.

A and *B*). An additional water-mediated salt bridge forms between Arg^{310} and $pThr^{345}$ (Fig. 1*B*). In unphosphorylated IRAK4, the majority of the activation loop is unresolved in the electron density map and therefore is most likely unstructured. The region of the activation segment immediately downstream of the DFG motif, Leu^{332}–Lys^{338}, assembles into a short α-helix (Fig. 1*A*). This α-helix packs into the remaining space vacated by the αC helix in the unphosphorylated conformation. Leu^{332}, which is solvent-facing in the active conformation, is relocated to the core of the N-lobe, occupying the space where the critical Glu^{233} residue would be in the active conformation (Fig. 1*B*). In the phosphorylated IRAK4 structure, the Asp^{329} side chain of the DFG motif faces outward toward the solvent (Fig. 1*C*). In the current unphosphorylated structure, Asp^{329} has flipped toward the active site, where it coordinates a Mg^{2+} ion (Fig. 1*C*). The side chain of Phe^{330} is flipped toward the αC helix, where it packs against Leu^{302}, Met^{237}, and Cys^{240} to fill a site occupied by Val^{236} on the αC helix in phosphorylated IRAK4 (Fig. 1*C*). Despite the conformational changes, the DFG motif of AMP-PNP–bound IRAK4 is still considered in a "DFG-in" conformation that is more similar to the DFG-in conformation of the active kinase state than the "DFG-out" conformation of a type II kinase inhibitor–bound state (35).

The assembly of the regulatory spine (R-spine) is a hallmark of kinase domains in the active conformation (20). The R-spine is a collection of four residues from the His–Arg–Asp (HRD) motif (RS1), the DFG motif (RS2), the αC helix (RS3), and the β4 strand (RS4). In the phosphorylated IRAK4 KD, the residues Leu^{248}, Met^{237}, Phe^{330}, and His^{309} align into a rigid hydrophobic column (Fig. S1*C*), indicative of an active conformation. In the unphosphorylated IRAK4 KD, the outward movement of the αC helix serves to displace the RS3 residue Met^{237} from the R-spine (Fig. 2*A*). The combined rearrangements of the DFG motif and the αC helix in the unphosphorylated conformation result in the disassembly of the R-spine, confirming that the kinase is in an inactive conformation (Fig. 2*A*). In the current unphosphorylated IRAK4 structure, Mg^{2+} ion coordination is also distinct, with a single ion interacting with all three phosphate groups of AMP-PNP (Fig. 2*B*). The movement of the Asp^{329} side chain of the DFG motif toward the active site facilitates its coordination of the Mg^{2+} ion (Figs. 1*B* and 2*B*). Asn^{316} makes an additional contact with the Mg^{2+}. Typically, an active, phosphorylated protein kinase requires two Mg^{2+} ions to catalyze the transfer of phosphate groups to substrate.

Unphosphorylated IRAK4^{KD} in complex with AMP-PNP adopts a CDK2/c-Src inactive kinase conformation that is αC-out

The conformation of the unphosphorylated IRAK4 KD closely resembles the "CDK2/c-Src" inactive kinase conformation previously observed in the crystal structures of c-Src (PDB code 2SRC) (36), Abl (PDB code 2G1T) (37), CDK2 (PDB code 1HCK) (38, 39), and EGFR bound to both lapatinib (PDB code 1XKK) (40) and AMP-PNP (PDB code 2GS7) (18). This inactive conformation is recognized as "αC-out" and has been exploited

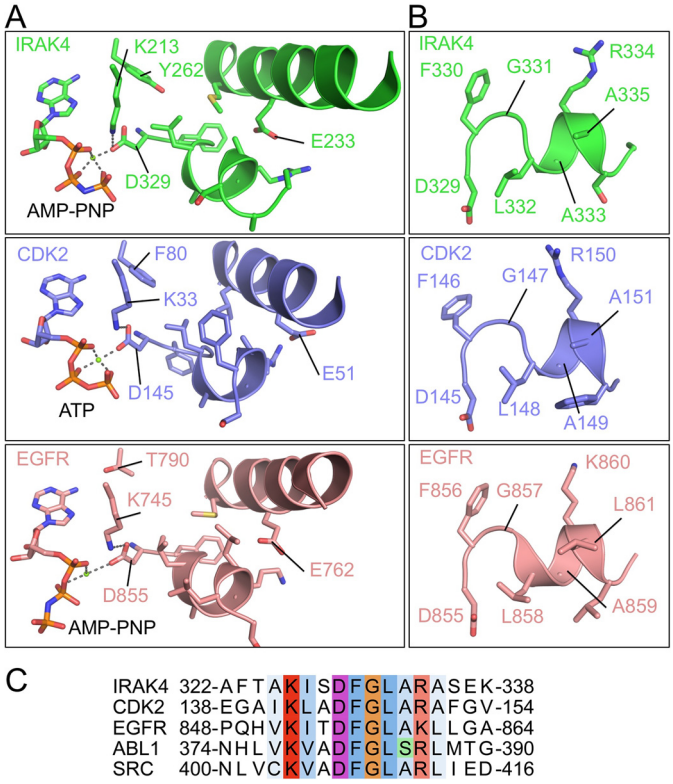

Figure 3. Comparison of the DFG motifs and inhibitory helices of IRAK4, CDK2, EGFR, ABL1, and SRC. *A*, comparison of the αC-helix and DFG motif conformations of ATP- or AMP-PNP–bound IRAK4 (*green*), CDK2 (*blue*, 1HCK), and EGFR (*pink*, 2GS7). *B*, comparison of the inhibitory helix conformation of ATP- or AMP-PNP–bound IRAK4 (*green*), CDK2 (*blue*, 1HCK), and EGFR (*pink*, 2GS7). *C*, sequence alignment of the DFG motif of IRAK4 with other kinases known to adopt the CDK2/c-Src–like inactive conformation.

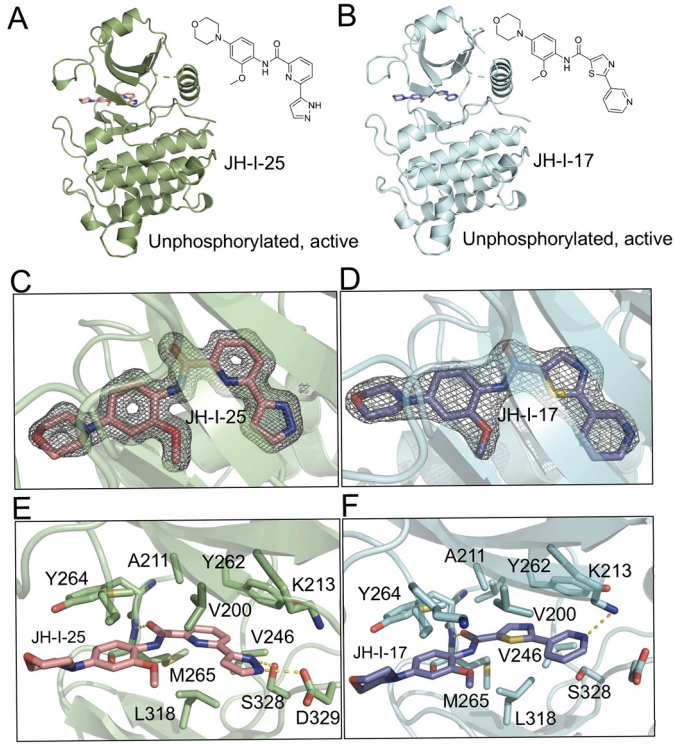

Figure 4. Unphosphorylated IRAK4 in complex with type I inhibitors. *A*, chemical structure and binding pose of the type I inhibitor JH-I-25 (*pink*, *sticks*) bound to unphosphorylated IRAK4 (*green*). *B*, chemical structure and binding pose of the type I inhibitor JH-I-17 (*blue*, *sticks*) bound to unphosphorylated IRAK4 (*cyan*). *C*, $2F_o - F_c$ electron density map within 1.5 Å of the ligand JH-I-25 contoured at 1.5 σ (colored as in *A*). *D*, $2F_o - F_c$ electron density map within 1.5 Å of the ligand JH-I-17 contoured at 1.5 σ (colored as in *B*). *E*, detailed interactions between IRAK4 and JH-I-25 (colored as in *A*). *F*, detailed interactions between IRAK4 and JH-I-17 (colored as in *B*).

for type I1/2 inhibitors such as lapatinib (35). Comparison of the current unphosphorylated IRAK4 KD bound to AMP-PNP with CDK2 and EGFR (in complex with ATP and AMP-PNP, respectively) shows a shared outward position of the αC helix (αC-out) (Fig. 3*A*). In all three kinases, the activation loop has assembled into a short inhibitory helix that packs into the active site, and the side-chain movement of the DFG Asp^{329} residue allows for the coordination of a single Mg^{2+} ion (Fig. 3*A*). The position of the Mg^{2+} ion is shared among all three kinases. These conformation-dependent differences in both the nucleotide conformation and Mg^{2+} coordination have been previously noted in both CDK2 (PDB code 1HCK) (39) and c-Src (PDB code 2SRC) (36). The DFG Asp residue also interacts with the catalytic lysine from strand β3 (Fig. 3*A*). In all three kinases, a rotation in the αC helix removes the critical glutamate residue from the active site. Instead, this αC glutamate points downwards toward the inhibitory helix (Fig. 3*A*). The overall conformation of the DFG motif and the inhibitory helix are closely shared among the inactive conformations of IRAK4, CDK2, and EGFR (Fig. 3*B*). Although IRAK4, c-Src, Abl, EGFR, and CDK2 are members of different kinase families (tyrosine kinase-like family for IRAK4; tyrosine kinase family for c-Src, Abl, and EGFR; and CDK, mitogen-activated protein kinase, glycogen synthase kinase, and CDK-like kinase family for CDK2), they all share sequence conservation past the DFG motif into the autoinhibitory helix (Fig. 3, *B* and *C*). The Leu and Ala residues immediately downstream of the DFG motif are conserved in all four kinases (with the exception of Abl, where Ala is replaced by a Ser), followed by a basic residue (Arg in IRAK4, c-Src, Abl, and CDK2; and Lys in EGFR) (Fig. 3*C*). The basic residue is thought to interact with and stabilize the negative charge of the αC glutamate in the inactive conformation. These data suggest that these residues may be critical for the stabilization of the inhibitory helix and this inactive conformation.

Unphosphorylated IRAK4 in complex with type I inhibitors adopts active kinase conformation that is DFG-in and αC-in

We next attempted to characterize the binding mode of inhibitors to unphosphorylated IRAK4. We chose two previously characterized inhibitors, JH-I-25 and JH-I-17, derived from a series of thiazole benzamide compounds (Fig. 4, *A* and *B*) for crystallization trials (41). KinomeScan analysis (42) of 1 μM JH-I-25 against a near-comprehensive panel of 456 kinases, most in phosphorylated or active forms, demonstrated good selectivity of this inhibitor for IRAK1 and IRAK4 (Fig. S2). The S-score of S(10) equals 0.04, which means that only 4% of 456 kinases showed above 90% inhibition. Crystals of $IRAK4^{KD\text{-}D311N}$ in complex with both inhibitors contain two $IRAK4^{KD\text{-}D311N}$ molecules in the asymmetric unit, and the structures were solved at 1.4 and 2.1 Å, respectively, for JH-I-25 and JH-I-17 (Table 1 and Fig. 4, *A* and *B*). The electron density maps allowed us to unambiguously place the compounds in the

active site (Fig. 4, *C* and *D*, and Fig. S1*C*). Although the kinase domain is unphosphorylated, IRAK4$^{KD\text{-}D311N}$ crystallized in the active conformation in complex with both inhibitors, confirming that JH-I-25 and JH-I-17 are type I inhibitors of IRAK4. Both compounds are planar aromatic heterocyclic molecules that interact with the hydrophobic surfaces of the ATP-binding pocket and with the hinge region through a single hydrogen bond between the inhibitor amide carbonyl and the backbone nitrogen of Met^{265} (Fig. 4, *E* and *F*). JH-I-25 makes additional hydrogen bonds between the pyrazole nitrogens and the side chain hydroxyl of Ser^{328} and carboxylic acid of Asp^{329} (Fig. 4*E*). In the JH-I-17 structure, the pyrazole ring is replaced with a pyridine ring. The pyridine nitrogen accepts a hydrogen bond from the catalytic Lys^{213} (Fig. 4*F*).

Screening against a type II inhibitor collection using unphosphorylated IRAK4

Identifying small molecule kinase inhibitors through traditional high-throughput screening typically uses highly active, activation loop-phosphorylated recombinant kinase domains at very low concentrations of ATP. Thus, the identified compounds are most likely type I inhibitors that interact with the active conformation of the ATP cleft. Type II kinase inhibitors and allosteric kinase inhibitors, which often prevent kinase action through selective binding to inactive conformations of kinases, could be missed under this kind of high-throughput screening condition. Because unphosphorylated WT IRAK4 kinase domain is dimeric in solution and therefore easily isolated from phosphorylated IRAK4 monomers (5), we set out to use unphosphorylated IRAK4 kinase dimers to identify unique IRAK4 inhibitors that potentially target an inactive conformation. Because of the availability of an in-house type II kinase inhibitor collection (130 compounds), we screened this collection using unphosphorylated IRAK4 kinase domain in a thermal shift assay (Table S1). A known ABL tyrosine kinase inhibitor, ponatinib (43), and an in-house compound, HG-12-6, were the top two hits from the screen. To check whether these two compounds bound to IRAK4 as type II inhibitors, a LanthaScreen Eu kinase-binding assay was used to compare the binding affinities of the compounds for unphosphorylated inactive IRAK4 kinase domain with those for the phosphorylated active IRAK4 kinase domain (Fig. 5*A*). Both ponatinib and HG-12-6 show preferential binding to unphosphorylated inactive IRAK4, suggesting that they may be indeed type II inhibitors of IRAK4.

Unphosphorylated IRAK4 in complex with type II inhibitors adopts inactive kinase conformation that is DFG-out

We determined co-crystal structures of the unphosphorylated WT IRAK4 kinase domain in complex with ponatinib and HG-12-6 at 2.3 and 2.5 Å resolutions, respectively (Table 1). The electron densities for the bound inhibitors were clearly visible in both omit maps and $2F_o - F_c$ maps (Fig. S3). Unlike type I inhibitors, ponatinib not only occupies the adenine pocket but also extends into an adjacent hydrophobic pocket (Fig. 5, *B–E*). This hydrophobic pocket is created by the DFG motif adopting a DFG-out conformation (Fig. 5, *B* and *E*). In this conformation, Asp^{329} of the DFG motif flips ~180° from the active conformation required for ATP phosphotransfer. This allows for Phe^{330} and Asp^{329} to effectively swap positions, opening up an allosteric hydrophobic pocket. Movement of Phe^{330} (RS2 of the R-spine) toward the ATP-binding cleft enables binding of the inhibitors to the hydrophobic pocket, resulting in R-spine disruption (Fig. 5*C*). Adoption of the DFG-out conformation and accompanied movement of the αC-helix confirm the type II nature of these inhibitors (Fig. 5, *D* and *E*). The conformation of the αC helix observed in the type II inhibitor bound DFG-out structure is distinct from the conformation observed in the AMP-PNP bound IRAK4 structure (Fig. 5*D*). Compared with the active conformation, the αC helix in the DFG-out conformation rotates away by ~12° along its axis, but maintains the salt-bridge interaction between Asp^{233} of the αC helix and the Lys^{213} of the β3 strand. In the αC-out conformation, the αC helix rotation is more significant and results in disruption of the salt-bridge interaction (Figs. 5*D* and 1*B*).

Structural comparison reveals that IRAK4 bound ponatinib adopts a conformation that is similar to its ABL-bound conformation (43), with an overall RMSD of 1.12 Å (Fig. 5*G*). However, there are also significant differences. As observed in its complex with ABL, the "head" of ponatinib occupies the adenine region, whereas ring A is located near the kinase gatekeeper residue (Tyr^{262}) and the ATP back hydrophobic pocket (Fig. 5*F*). Ponatinib was developed to overcome the imatinib resistance conferred by the BCR-ABL gatekeeper T315I mutation, in which the linear carbon– triple bond allows the compound to fit past the bulky Ile side chain into the kinase hydrophobic pocket. IRAK4 has a Tyr (Tyr^{262}) as the gatekeeper residue, a feature unique to the IRAK kinase family. To accommodate the bulky Tyr^{262} side chain in IRAK4, ring A of ponatinib rotates outward by ~25°, resulting in slightly outward displacement of the head of ponatinib from the adenine binding region, leading to a suboptimal interaction in this pocket. Simultaneously, the ring A rotation enables a unique π–π interaction with the gatekeeper Tyr^{262} of IRAK4 (Fig. 5, *F* and *G*). The amide linkage of ponatinib forms hydrogen bonds with the main chain of Asp^{329} from the DFG loop and with the Glu^{233} side chain from helix αC. The CF3 substituted ring B mostly engages IRAK4 through hydrophobic interactions, and the "tail" methylpiperazine group forms hydrogen bonds with IRAK4 main-chain atoms.

Our in-house compound HG-12-6 has a similar chemical scaffold as ponatinib (Fig. 5*A*). The most differentiating components are the head of the inhibitor and the lack of a methyl substituent on ring A. Because replacement of the head group in HG-12-6 retained similar inhibitory activity, we argue that alternative hinge-binding groups could be developed to replace the original head from ponatinib to achieve specificity. However, high-affinity inhibitors likely require planar geometry in the head group to fit in the adenine-binding region. Without the methyl substituent on ring A, the entire HG-12-6 molecule shifts inward to the ATP pocket compared with the binding mode of ponatinib (Fig. S4).

Discussion

Understanding the conformational changes that occur during IRAK4 activation is essential for elucidating a comprehensive molecular mechanism. We have demonstrated that unphosphorylated IRAK4 can adopt both the active conformation and

multiple inactive conformations. It is likely that ligand binding affects the conformational equilibrium of IRAK4. Because unphosphorylated IRAK4 could be crystallized in both an active conformation (when bound to JH-I-25 and JH-I-17) and multiple distinct inactive conformations (when bound to AMP-PNP, ponatinib, or HG-12-6), we hypothesize that ligand binding promotes the adoption of a predominant conformation, enabling growth of well-diffracting crystals. In solution, it is probable that IRAK4 can readily adopt both the inactive and active conformations and may exist in a dynamic equilibrium between the two states. Whether IRAK4 prefers one conformation to another in the absence of ligand is unclear. Further experiments are needed to understand the conformational dynamics of IRAK4.

Development of protein-kinase inhibitors has long been a major focus of the pharmaceutical industry, but identifying

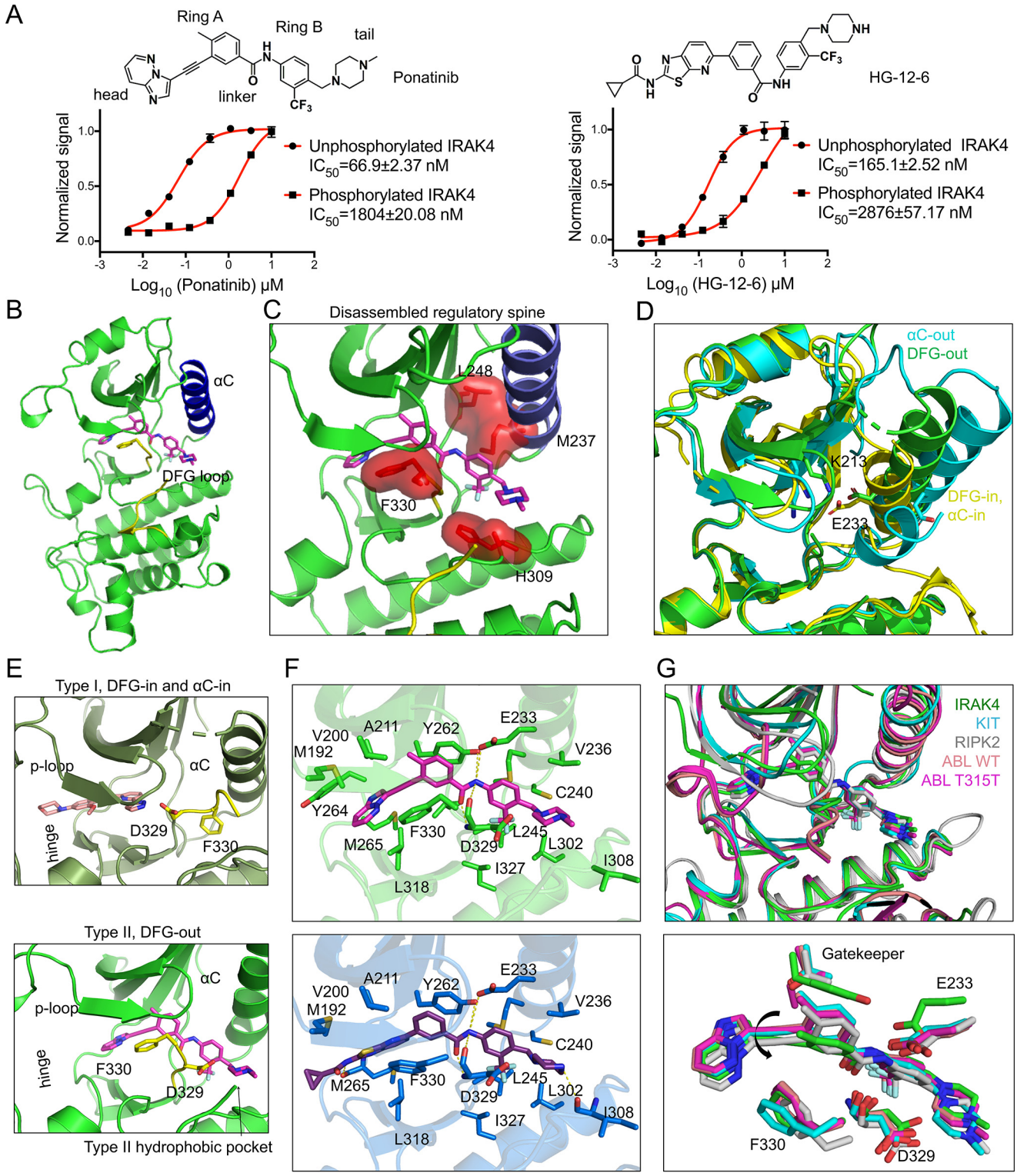

compounds with sufficient selectivity to achieve an acceptable therapeutic index has been challenging. The high conservation of residues that form the ATP-binding pocket makes developing selective ATP competitive inhibitors difficult. However, it has been recognized that compounds exploiting the more structurally distinct inactive conformations of individual protein kinases could achieve both high potency and high specificity (35). The inactive conformation of AMP-PNP–bound IRAK4 has been characterized as an αC-out inactive conformation, which is targeted by type I1/2 inhibitors (35). These inhibitors occupy the ATP-binding pocket and extend to the adjacent hydrophobic pocket opened by the rotation of the αC helix. Lapatinib is an U.S. Food and Drug Administration–approved type I1/2 EGFR inhibitor with the αC-out configuration. When lapatinib-bound EGFR is superimposed to AMP-PNP bound IRAK4, it clearly shows that the Tyr^{262} gatekeeper residue blocks lapatinib for access to the adjacent back pocket in IRAK4 (Fig. S5). Therefore, a bulky gatekeeper of IRAK4 appears to render the back hydrophobic pocket inaccessible to type I1/2 inhibitor binding.

In the type II conformation with DFG-out, the narrow entrance to the back hydrophobic pocket is reopened by flipping Asp^{329} in the DFG motif away while keeping Tyr^{262} in place (Fig. S5), suggesting that IRAK4 can potentially be a suitable target for type II kinase inhibitors. Indeed, we screened and identified type II inhibitors for unphosphorylated IRAK4 and determined two such crystal structures, which revealed the binding into the back hydrophobic pocket and adoption of a type II mode of interaction. In this regard, CDK8, which has a Phe gatekeeper, was co-crystallized with the type II inhibitor sorafenib (PDB code 3RGF), demonstrating that the presence of a bulky aromatic gatekeeper does not preclude the binding of a type II inhibitor (44). Whereas IRAK kinases share the conserved Tyr gatekeeper residue, the back hydrophobic pockets in different IRAKs are variable. Therefore, our studies extend our understanding on the IRAK4 kinase and uncover the possibility of its selective inhibition by type II inhibitors.

Experimental procedures

Protein expression and purification

Expression and purification of IRAK4 was conducted as described previously (5). Briefly, PCR fragments of human IRAK4 kinase domain ($IRAK4^{KD}$, 164–460) were inserted into pFastBacHTB between BamHI and NotI restriction sites. The IRAK4 D311N mutation ($IRAK4^{KD\text{-}D311N}$) was introduced using the QuikChange II site-directed mutagenesis kit (Agilent Technologies). Plasmids were transformed into DH10Bac™ *Escherichia coli* competent cells followed by bacmid purification using the Bac-to-Bac® baculoviral expression system. Bacmids were transfected into Sf9 monolayer cells to generate baculoviruses. Harvested baculoviruses were used to infect High Five™ cells for 48 h at 27 °C. The cells were harvested by centrifugation and resuspended in lysis buffer containing 50 mM Hepes-NaOH, pH 7.5, 300 mM NaCl, 10 mM imidazole, and 1 mM tris(2-carboxyethyl)phosphine–HCl. DNase (10 μg/ml) and protease inhibitors (SIGMAFAST™ protease inhibitor mixture tablets, EDTA-free) were added to the lysate. The cells were lysed with an Avestin EmulsiFlex-*C3* homogenizer. Cell debris was cleared via centrifugation at 48,400 relative centrifugal force. Clarified lysates were incubated with HisPur™ cobalt resin and washed extensively with lysis buffer. Bound proteins were eluted with lysis buffer supplemented with 150 mM imidazole. The eluates were subjected to N-terminal His_6 tag cleavage and dephosphorylation using overnight incubation with His-tagged tobacco etch virus protease, His-tagged λ-phosphatase and 5 mM $MnCl_2$ at 4 °C. IRAK4 was then further purified with anion exchange chromatography using Source 15Q resin and a final size-exclusion chromatography step using a Superdex 200 10/30 GL equilibrated in 20 mM Hepes-NaOH at pH 7.5, 150 mM NaCl and 1 mM tris(2-carboxyethyl)phosphine–HCl. Fractions containing IRAK4 were pooled, concentrated, and flash frozen in liquid N_2. To generate phosphorylated $IRAK4^{KD}$, WT $IRAK4^{KD}$ was incubated with 5 mM ATP and 10 mM $MgCl_2$ for 4 h at 25 °C after elution from cobalt beads and further purified by anion-exchange and size-exclusion chromatography.

Type II inhibitor screening using a thermal shift assay

Purified dephosphorylated $IRAK4^{KD}$ was used to screen an in-house type II inhibitor collection (130 compounds). Compounds at 25 μM were mixed with 3 μM $IRAK4^{KD}$ and 1-fold protein thermal shift dye (Thermo Fisher Scientific) in a 20-μl reaction volume. Thermal scanning (25–75 °C at 1.5 °C/min) was performed, and melting curves were recorded on StepOne RT-PCR machine. Data analysis was done by Protein Thermal Shift™ software (Thermo Fisher Scientific).

Crystallization and structure determination

$IRAK4^{KD\text{-}D311N}$ at 10 mg/ml was incubated with AMP-PNP at a 10:1 molar ratio prior to setting up crystallization trays. The crystals were obtained by hanging-drop vapor diffusion at 16–20 °C by mixing equal volumes of protein and reservoir

Figure 5. IRAK4 in complex with type II inhibitors. *A*, chemical structures of the type II inhibitors identified in screen and used in the co-crystallization. The affinities of two type II inhibitors to unphosphorylated and phosphorylated IRAK4 kinase domain were measured by LanthaScreen Eu kinase-binding assay. Both ponatinib and HG-12-6 showed preferred binding to unphosphorylated IRAK4 kinase domain. *B*, a *ribbon diagram* showing the overview of IRAK4 in complex with ponatinib. The αC-helix is colored in *blue*, and the DFG loop is colored in *yellow*. Ponatinib is shown in a *stick model* and colored in *magenta*. *C*, type II inhibitor binding to a DFG-out conformation of IRAK4, showing disrupted regulatory spine of IRAK4 (colored as in *B*). Residues forming the regulatory spine are shown as *red sticks* and highlighted with *red surface*. *D*, comparison of the αC-helix position and conserved salt-bridge interaction between Glu^{233} and Lys^{213} in active IRAK4 (DFG-in and αC-in, *yellow*, PDB code 2OID), inactive IRAK4 in complexes with AMP-PNP (αC-out, *cyan*) and inactive IRAK4 in complexes with ponatinib (DFG-out, *green*). *E*, ribbon diagrams comparing DFG-in active conformation in IRAK4 (*cartoon*, *olive green*) bound to JH-I-25 (*sticks*, *pink*, *top panel*) and DFG-out inactive conformation in IRAK4 (*cartoon*, *green*) bound to ponatinib (*sticks*, *magenta*, *bottom panel*). In these two conformations, Asp^{329} and Phe^{330} swap positions with accompanied movement of the αC-helix. *F*, detailed interaction between IRAK4 (*green*) with ponatinib (*magenta*) and between IRAK4 (*blue*) with HG-12-6 (*dark purple*). *G*, superimposition of ponatinib bound IRAK4 structure with reported kinase structures in complex with ponatinib (PDB code of ABL, 3OXZ; PDB code of ABL T315I, 3IK3; PDB code of KIT, 4U0I; and PDB code of RIPK2, 4C8B). These kinases share the conserved DFG-out conformation. The rotation of ring A of ponatinib appears to accommodate the different sizes of gatekeeper residues.

solution (1.6–1.9 M ammonium sulfate, 100 mM Hepes-NaOH, pH 7.0). Crystals were harvested, cryoprotected with reservoir solution supplemented with 20% (v/v) ethylene glycol, and flash frozen in liquid nitrogen. Native data collection was performed at Argonne National Laboratory using the Advanced Photon Source Beamline 24-ID-C. Crystals of $IRAK4^{KD\text{-}D311N}$ with type I kinase inhibitors were obtained by co-crystallization with a 5:1 molar excess of JH-I-17 and JH-I-25 in 150 mM DL-Malic acid and 20% PEG3350. Data collection was performed at National Synchrotron Light Source Beamlines X25A and X4A. Crystals of $IRAK4^{KD}$ with type II kinase inhibitors were obtained by co-crystallization with a 5:1 molar excess of HG-12-6 and ponatinib in 0.1 M Tris-HCl, pH 8.0, 20 mM cobalt chloride, and 1.5–1.6 M ammonium sulfate. Data collection was performed at Advanced Photon Source Beamlines 24-ID-C and 24-ID-E. All data reduction was accomplished with XDS/XSCALE (21) and solved by molecular replacement using Phenix (22). Model building and refinement were done with Coot (23) and Phenix (22). The figures were generated using PyMOL (24). Ramachandran statistics was calculated using Procheck (25).

Kinase-binding assay of IRAK4

LanthaScreen Eu kinase binding assay was used to compare binding affinities of dephosphorylated and phosphorylated IRAK4 to type II kinase inhibitors HG-12-6 and ponatinib identified from the inhibitor screening. In a 384-well plate format, 10 nM His-tagged dephosphorylated or phosphorylated $IRAK4^{KD}$ was preincubated with ponatinib or HG-12-6 in a kinase buffer (50 mM Hepes-NaOH, pH 7.5, 50 mM $NaCl_2$, 10 mM $MgCl_2$, 0.01% Tween 20, and 0.1% BSA) for 30 min at room temperature. 2 nM Eu–anti-His tag antibody (Invitrogen) and 250 nM ATP-competitive kinase inhibitor (kinase tracer 222) were then added to the protein-compound mixture. Time-resolved FRET signals were recorded on EnVision plate reader after 2 h of incubation, and the data were analyzed in GraphPad Prism 7.0.

Author contributions—L. W., R. F., and H. W. conceptualization; L. W., R. F., and Q. L. data curation; L. W. and R. F. formal analysis; L. W. and R. F. validation; L. W., R. F., and H. W. investigation; L. W. and R. F. visualization; L. W., R. F., and H. W. methodology; L. W., R. F., and H. W. writing-original draft; L. W., R. F., and H. W. writing-review and editing; J. M. H., H. G. C., S. J. B., and N. S. G. resources; H. W. supervision; H. W. funding acquisition.

Acknowledgments—We thank Dr. Qun Liu for collecting data of IRAK4 bound to JH-I-25. The Pilatus 6M detector on 24-ID-C beam line is funded by NIH-ORIP HEI Grant S10 RR029205. This research used resources of the Advanced Photon Source, a U.S. Department of Energy Office of Science User Facility operated for the Department of Energy Office of Science by Argonne National Laboratory under Contract DE-AC02-06CH11357. This work was partially based upon research conducted at the Northeastern Collaborative Access Team Beamlines, which are funded by NIGMS, National Institutes of Health Grant P41 GM103403.

References

1. Kawai, T., and Akira, S. (2010) The role of pattern-recognition receptors in innate immunity: update on Toll-like receptors. *Nat. Immunol.* **11,** 373–384 CrossRef Medline
2. Garlanda, C., Dinarello, C. A., and Mantovani, A. (2013) The interleukin-1 family: back to the future. *Immunity* **39,** 1003–1018 CrossRef Medline
3. Lin, S. C., Lo, Y. C., and Wu, H. (2010) Helical assembly in the MyD88-IRAK4-IRAK2 complex in TLR/IL-1R signalling. *Nature* **465,** 885–890 CrossRef Medline
4. Motshwene, P. G., Moncrieffe, M. C., Grossmann, J. G., Kao, C., Ayaluru, M., Sandercock, A. M., Robinson, C. V., Latz, E., and Gay, N. J. (2009) An oligomeric signaling platform formed by the Toll-like receptor signal transducers MyD88 and IRAK-4. *J. Biol. Chem.* **284,** 25404–25411 CrossRef Medline
5. Ferrao, R., Zhou, H., Shan, Y., Liu, Q., Li, Q., Shaw, D. E., Li, X., and Wu, H. (2014) IRAK4 dimerization and *trans*-autophosphorylation are induced by myddosome assembly. *Mol. Cell* **55,** 891–903 CrossRef Medline
6. Napetschnig, J., and Wu, H. (2013) Molecular basis of NF-κB signaling. *Annu. Rev. Biophys.* **42,** 443–468 CrossRef Medline
7. Kim, T. W., Staschke, K., Bulek, K., Yao, J., Peters, K., Oh, K. H., Vandenburg, Y., Xiao, H., Qian, W., Hamilton, T., Min, B., Sen, G., Gilmour, R., and Li, X. (2007) A critical role for IRAK4 kinase activity in Toll-like receptor-mediated innate immunity. *J. Exp. Med.* **204,** 1025–1036 CrossRef Medline
8. Lye, E., Dhanji, S., Calzascia, T., Elford, A. R., and Ohashi, P. S. (2008) IRAK-4 kinase activity is required for IRAK-4-dependent innate and adaptive immune responses. *Eur. J. Immunol.* **38,** 870–876 CrossRef Medline
9. von Bernuth, H., Picard, C., Puel, A., and Casanova, J. L. (2012) Experimental and natural infections in MyD88- and IRAK-4-deficient mice and humans. *Eur. J. Immunol.* **42,** 3126–3135 CrossRef Medline
10. von Bernuth, H., Picard, C., Jin, Z., Pankla, R., Xiao, H., Ku, C. L., Chrabieh, M., Mustapha, I. B., Ghandil, P., Camcioglu, Y., Vasconcelos, J., Sirvent, N., Guedes, M., Vitor, A. B., Herrero-Mata, M. J., *et al.* (2008) Pyogenic bacterial infections in humans with MyD88 deficiency. *Science* **321,** 691–696 CrossRef Medline
11. Cameron, B., Tse, W., Lamb, R., Li, X., Lamb, B. T., and Landreth, G. E. (2012) Loss of interleukin receptor-associated kinase 4 signaling suppresses amyloid pathology and alters microglial phenotype in a mouse model of Alzheimer's disease. *J. Neurosci.* **32,** 15112–15123 CrossRef Medline
12. Kim, T. W., Febbraio, M., Robinet, P., Dugar, B., Greene, D., Cerny, A., Latz, E., Gilmour, R., Staschke, K., Chisolm, G., Fox, P. L., DiCorleto, P. E., Smith, J. D., and Li, X. (2011) The critical role of IL-1 receptor-associated kinase 4-mediated NF-κB activation in modified low-density lipoprotein-induced inflammatory gene expression and atherosclerosis. *J. Immunol.* **186,** 2871–2880 CrossRef Medline
13. Koziczak-Holbro, M., Littlewood-Evans, A., Pöllinger, B., Kovarik, J., Dawson, J., Zenke, G., Burkhart, C., Müller, M., and Gram, H. (2009) The critical role of kinase activity of interleukin-1 receptor-associated kinase 4 in animal models of joint inflammation. *Arthritis Rheum.* **60,** 1661–1671 CrossRef Medline
14. Ngo, V. N., Young, R. M., Schmitz, R., Jhavar, S., Xiao, W., Lim, K. H., Kohlhammer, H., Xu, W., Yang, Y., Zhao, H., Shaffer, A. L., Romesser, P., Wright, G., Powell, J., Rosenwald, A., *et al.* (2011) Oncogenically active MYD88 mutations in human lymphoma. *Nature* **470,** 115–119 CrossRef Medline
15. Treon, S. P., Xu, L., Yang, G., Zhou, Y., Liu, X., Cao, Y., Sheehy, P., Manning, R. J., Patterson, C. J., Tripsas, C., Arcaini, L., Pinkus, G. S., Rodig, S. J., Sohani, A. R., Harris, N. L., *et al.* (2012) MYD88 L265P somatic mutation in Waldenstrom's macroglobulinemia. *N. Engl. J. Med.* **367,** 826–833 CrossRef Medline
16. Hu, J., Stites, E. C., Yu, H., Germino, E. A., Meharena, H. S., Stork, P. J. S., Kornev, A. P., Taylor, S. S., and Shaw, A. S. (2013) Allosteric activation of functionally asymmetric RAF kinase dimers. *Cell* **154,** 1036–1046 CrossRef Medline

17. Jeffrey, P. D., Russo, A. A., Polyak, K., Gibbs, E., Hurwitz, J., Massagué, J., and Pavletich, N. P. (1995) Mechanism of CDK activation revealed by the structure of a cyclinA–CDK2 complex. *Nature* **376,** 313–320 CrossRef Medline
18. Zhang, X., Gureasko, J., Shen, K., Cole, P. A., and Kuriyan, J. (2006) An allosteric mechanism for activation of the kinase domain of epidermal growth factor receptor. *Cell* **125,** 1137–1149 CrossRef Medline
19. Shan, Y., Arkhipov, A., Kim, E. T., Pan, A. C., and Shaw, D. E. (2013) Transitions to catalytically inactive conformations in EGFR kinase. *Proc. Natl. Acad. Sci. U.S.A.* **110,** 7270–7275 CrossRef Medline
20. Taylor, S. S., and Kornev, A. P. (2011) Protein kinases: evolution of dynamic regulatory proteins. *Trends Biochem. Sci.* **36,** 65–77 CrossRef Medline
21. Kabsch, W. (2010) XDS. *Acta Crystallogr. D Biol. Crystallogr.* **66,** 125–132 CrossRef Medline
22. Adams, P. D., Afonine, P. V., Bunkóczi, G., Chen, V. B., Davis, I. W., Echols, N., Headd, J. J., Hung, L. W., Kapral, G. J., Grosse-Kunstleve, R. W., McCoy, A. J., Moriarty, N. W., Oeffner, R., Read, R. J., Richardson, D. C., *et al.* (2010) PHENIX: a comprehensive Python-based system for macromolecular structure solution. *Acta Crystallogr. D Biol. Crystallogr.* **66,** 213–221 CrossRef Medline
23. Emsley, P., and Cowtan, K. (2004) Coot: model-building tools for molecular graphics. *Acta Crystallogr. D Biol. Crystallogr.* **60,** 2126–2132 CrossRef Medline
24. Delano, W. L. (2012) The PyMOL Molecular Graphics System, version 1.5.0.1, Schroedinger, LLC, New York
25. Laskowski, R. A., MacArthur, M. W., Moss, D. S., and Thornton, J. M. (1993) PROCHECK: a program to check the stereochemical quality of protein structures. *J. Appl. Cryst.* **26,**
26. Wang, Z., Liu, J., Sudom, A., Ayres, M., Li, S., Wesche, H., Powers, J. P., and Walker, N. P. (2006) Crystal structures of IRAK-4 kinase in complex with inhibitors: a serine/threonine kinase with tyrosine as a gatekeeper. *Structure* **14,** 1835–1844 CrossRef Medline
27. Kuglstatter, A., Villaseñor, A. G., Shaw, D., Lee, S. W., Tsing, S., Niu, L., Song, K. W., Barnett, J. W., and Browner, M. F. (2007) Cutting edge: IL-1 receptor-associated kinase 4 structures reveal novel features and multiple conformations. *J. Immunol.* **178,** 2641–2645 CrossRef Medline
28. Lee, K. L., Ambler, C. M., Anderson, D. R., Boscoe, B. P., Bree, A. G., Brodfuehrer, J. I., Chang, J. S., Choi, C., Chung, S., Curran, K. J., Day, J. E., Dehnhardt, C. M., Dower, K., Drozda, S. E., Frisbie, R. K., *et al.* (2017) Discovery of clinical candidate 1-{[(2*S*,3*S*,4*S*)-3-ethyl-4-fluoro-5-oxopyrrolidin-2-yl]methoxy}-7-methoxyisoquinoli ne-6-carboxamide (PF-06650833), a potent, selective inhibitor of interleukin-1 receptor associated kinase 4 (IRAK4), by fragment-based drug design. *J. Med. Chem.* **60,** 5521–5542 CrossRef Medline
29. Hanisak, J., Seganish, W. M., McElroy, W. T., Tang, H., Zhang, R., Tsui, H. C., Fischmann, T., Tulshian, D., Tata, J., Sondey, C., Devito, K., Fossetta, J., Garlisi, C. G., Lundell, D., and Niu, X. (2016) Efforts towards the optimization of a bi-aryl class of potent IRAK4 inhibitors. *Bioorg. Med. Chem. Lett.* **26,** 4250–4255 CrossRef Medline
30. Seganish, W. M., Fischmann, T. O., Sherborne, B., Matasi, J., Lavey, B., McElroy, W. T., Tulshian, D., Tata, J., Sondey, C., Garlisi, C. G., Devito, K., Fossetta, J., Lundell, D., and Niu, X. (2015) Discovery and structure enabled synthesis of 2,6-diaminopyrimidin-4-one IRAK4 inhibitors. *ACS Med. Chem. Lett.* **6,** 942–947 CrossRef Medline
31. Lim, J., Altman, M. D., Baker, J., Brubaker, J. D., Chen, H., Chen, Y., Fischmann, T., Gibeau, C., Kleinschek, M. A., Leccese, E., Lesburg, C., Maclean, J. K., Moy, L. Y., Mulrooney, E. F., Presland, J., *et al.* (2015) Discovery of 5-amino-*N*-(^{1}H-pyrazol-4-yl)pyrazolo[1,5-a]pyrimidine-3-carboxamide inhibitors of IRAK4. *ACS Med. Chem. Lett.* **6,** 683–688 CrossRef Medline
32. McElroy, W. T., Michael Seganish, W., Jason Herr, R., Harding, J., Yang, J., Yet, L., Komanduri, V., Prakash, K. C., Lavey, B., Tulshian, D., Greenlee, W. J., Sondey, C., Fischmann, T. O., and Niu, X. (2015) Discovery and hit-to-lead optimization of 2,6-diaminopyrimidine inhibitors of interleukin-1 receptor-associated kinase 4. *Bioorg. Med. Chem. Lett.* **25,** 1836–1841 CrossRef Medline
33. McElroy, W. T., Tan, Z., Ho, G., Paliwal, S., Li, G., Seganish, W. M., Tulshian, D., Tata, J., Fischmann, T. O., Sondey, C., Bian, H., Bober, L., Jackson, J., Garlisi, C. G., Devito, K., *et al.* (2015) Potent and selective amidopyrazole inhibitors of IRAK4 that are efficacious in a rodent model of inflammation. *ACS Med. Chem. Lett.* **6,** 677–682 CrossRef Medline
34. Smith, G. F., Altman, M. D., Andresen, B., Baker, J., Brubaker, J. D., Chen, H., Chen, Y., Childers, M., Donofrio, A., Ferguson, H., Fischer, C., Fischmann, T. O., Gibeau, C., Hicks, A., Jin, S., *et al.* (2017) Identification of quinazoline based inhibitors of IRAK4 for the treatment of inflammation. *Bioorg. Med. Chem. Lett.* **27,** 2721–2726 CrossRef Medline
35. Roskoski, R., Jr. (2016) Classification of small molecule protein kinase inhibitors based upon the structures of their drug-enzyme complexes. *Pharmacol. Res.* **103,** 26–48 CrossRef Medline
36. Xu, W., Doshi, A., Lei, M., Eck, M. J., and Harrison, S. C. (1999) Crystal structures of c-Src reveal features of its autoinhibitory mechanism. *Mol. Cell* **3,** 629–638 CrossRef Medline
37. Levinson, N. M., Kuchment, O., Shen, K., Young, M. A., Koldobskiy, M., Karplus, M., Cole, P. A., and Kuriyan, J. (2006) A Src-like inactive conformation in the abl tyrosine kinase domain. *PLoS Biol.* **4,** e144 CrossRef Medline
38. Schulze-Gahmen, U., De Bondt, H. L., and Kim, S. H. (1996) High-resolution crystal structures of human cyclin-dependent kinase 2 with and without ATP: bound waters and natural ligand as guides for inhibitor design. *J. Med. Chem.* **39,** 4540–4546 CrossRef Medline
39. De Bondt, H. L., Rosenblatt, J., Jancarik, J., Jones, H. D., Morgan, D. O., and Kim, S. H. (1993) Crystal structure of cyclin-dependent kinase 2. *Nature* **363,** 595–602 CrossRef Medline
40. Wood, E. R., Truesdale, A. T., McDonald, O. B., Yuan, D., Hassell, A., Dickerson, S. H., Ellis, B., Pennisi, C., Horne, E., Lackey, K., Alligood, K. J., Rusnak, D. W., Gilmer, T. M., and Shewchuk, L. (2004) A unique structure for epidermal growth factor receptor bound to GW572016 (lapatinib): relationships among protein conformation, inhibitor off-rate, and receptor activity in tumor cells. *Cancer Res.* **64,** 6652–6659 CrossRef Medline
41. Buckley, G. M., Gowers, L., Higueruelo, A. P., Jenkins, K., Mack, S. R., Morgan, T., Parry, D. M., Pitt, W. R., Rausch, O., Richard, M. D., Sabin, V., and Fraser, J. L. (2008) IRAK-4 inhibitors: a series of amides. *Bioorg. Med. Chem. Lett.* **18,** 3211–3214 CrossRef Medline
42. Davis, M. I., Hunt, J. P., Herrgard, S., Ciceri, P., Wodicka, L. M., Pallares, G., Hocker, M., Treiber, D. K., and Zarrinkar, P. P. (2011) Comprehensive analysis of kinase inhibitor selectivity. *Nat. Biotechnol.* **29,** 1046–1051 CrossRef Medline
43. O'Hare, T., Shakespeare, W. C., Zhu, X., Eide, C. A., Rivera, V. M., Wang, F., Adrian, L. T., Zhou, T., Huang, W. S., Xu, Q., Metcalf, C. A., 3rd, Tyner, J. W., Loriaux, M. M., Corbin, A. S., Wardwell, S., *et al.* (2009) AP24534, a pan-BCR-ABL inhibitor for chronic myeloid leukemia, potently inhibits the T315I mutant and overcomes mutation-based resistance. *Cancer Cell* **16,** 401–412 CrossRef Medline
44. Schneider, E. V., Böttcher, J., Blaesse, M., Neumann, L., Huber, R., and Maskos, K. (2011) The structure of CDK8/CycC implicates specificity in the CDK/cyclin family and reveals interaction with a deep pocket binder. *J. Mol. Biol.* **412,** 251–266 CrossRef Medline

Conformational flexibility and inhibitor binding to unphosphorylated interleukin-1 receptor –associated kinase 4 (IRAK4)

Li Wang, Ryan Ferrao, Qiubai Li, John M. Hatcher, Hwan Geun Choi, Sara J. Buhrlage, Nathanael S. Gray and Hao Wu

J. Biol. Chem. 2019, 294:4511-4519.
doi: 10.1074/jbc.RA118.005428 originally published online January 24, 2019